Pressure and Noise Estimation of Tandem Cylinder Flow Based on PIV

Langsheng Chen[1] and Qingqing Ye[1,*]

1 Key Laboratory of Fluid Power and Mechatronic Systems, Department of Mechanics,
Zhejiang University, Hangzhou 310027, China
*Corresponding author email: qingqing_ye@zju.edu.cn
Keywords: PIV, POD denoising, pressure reconstruction, tandem cylinder

ABSTRACT

The present work proposes an optimized method for pressure reconstruction and far-field noise prediction for tandem cylinder flow based on time-resolved planar particle image velocimetry (PIV). Proper orthogonal decomposition (POD) low-order reconstruction is applied to mitigate the incoherent noise introduced during PIV measurement and processing and enhances the identification of dynamic characteristics of relative structures within the flow field. As a result, PIV-based pressure reconstruction through solving the Poisson equation encompasses fewer errors arising from contaminated boundary conditions and Poisson source terms, thereby mitigating the propagation of errors into pressure. The time-marching algorithm accelerates the convergence and stabilizes the iterative progress while solving the Poisson equation, leading a considerable computation savings for cases with multiple snapshots like aeroacoustics relative investigation. The reconstructed wall pressure is compared with the reference pressure fluctuation signal simultaneously measured, yielding good agreement. Finally, the far-field noise was predicted through Curle's analogy based on reconstructed wall pressure, considering the spanwise correction derived through an additional spanwise planar PIV. The predicted far-field noise agrees well with the reference microphone measurement. The overall assessment demonstrates that the employment of POD low-order reconstruction and time-marching algorithm significantly improve the speed and accuracy for estimating pressure field and far-field noise.

1. Introduction

Pressure fluctuations over the solid surface is a key aerodynamic parameter and play a significant role in noise generation and structural vibration. The recent development of particle image velocimetry (PIV) provides direct access to extract pressure information from the instantaneous velocity database, enabling a non-intrusive and whole-field measurement for velocity and pressure simultaneously (van Oudheusden, 2013). Particularly, the time-resolved PIV (TR-PIV) offers high-temporal and -spatial resolution to estimate instantaneous pressure, enabling the investigations of dynamic behavior of turbulent boundary layer (S. Ghaemi & Scarano, 2013) and aeroacoustic problems (Zhang, Sciacchitano, & Pröbsting, 2018). As a result, the unsteady flow

behavior responsible for the pressure fluctuations and noise generation can be interpolated with an individual PIV measurement.

Generally, for PIV-based pressure reconstruction, the pressure gradient ∇P is usually derived from the instantaneous velocity field based on the incompressible Navier-Stokes equation (1):

$$\nabla P = -\rho \frac{DU}{Dt} + \mu \nabla^2 U \quad (1)$$

where DU/Dt is the material acceleration, ρ is the fluid density, U is the instantaneous velocity and μ is the dynamic viscosity. Both Eulerian and Lagrangian approaches are used to calculate material acceleration (van Oudheusden, 2013). The former divides material acceleration into local and advective acceleration, which could be derived from temporal and spatial derivatives of velocity. The latter needs a trajectory reconstruction of a 'fluid parcel' over time to calculate the temporal derivative of velocity. The Eulerian approach performs better for rotational flow (R. de Kat & van Oudheusden, 2011) and offers a straightforward link to the PIV velocity grid, simplifying the extract of pressure gradients from velocity (van Oudheusden, 2013).

The second step is to determine pressure through directly spatial integrating pressure gradient or solving the Poisson equation. Generally, direct spatial integrating suffers from accumulating errors from velocity along the integration path, while solving the Poisson equation inherently diffuses errors globally (van Oudheusden, 2013). However, errors in the velocity field can contaminate the Poisson source term and boundaries, thereby deteriorating pressure (Pan, Whitehead, Thomson, & Truscott, 2016). Particularly, boundaries of measurement domain are most sensitive to velocity errors, demonstrating by Auteri (2015) through Monte Carlo analysis, that its associated errors require careful attention. And pretreatment for velocity denoising is necessary for accurate pressure reconstruction.

Not only suffers from error propagation, solving the Poisson equation approach also faces expensive computational costs. To achieve an acceptable convergence, a large number of iterations is indispensable for a specific iterative algorithm. By applying Successive Over Relaxation (SOR) scheme in the Poisson solver (Fujisawa, Tanahashi, & Srinivas, 2005), which introduces a relaxation factor β ($1 < \beta < 2$) weighting average between the previous and updated values, the computational burden is alleviated. However, facing high-frequency and large samples database (D. Ragni, Avallone, van der Velden, & Casalino, 2018), the computational cost is still non-negligible. Enhancing β towards 2 can speed up convergence but leads to instability or even divergence of iterations. Fewer iterations are sufficient for convergence when the initial guess is very similar to the solution. Therefore, we propose the time-marching algorithm, where the initial guess is given by the solution of the Poisson equation at the previous instant. This is physically reasonable because the time interval between two instants is small for TR-PIV, leading to minimal dynamic evolutions. Meanwhile, the iterative progress is stabilized so that larger β is available,

thus again accelerating computation. After the spatial pressure has been reconstructed, the wall pressure is evaluated by integrating from the nearest nodes coincided with the PIV grid (Jux, Sciacchitano, & Scarano, 2020). Then, the wall pressure is input into Curle's analogy to predict far-field noise (Zhang et al., 2018).

The present study aims to evaluate the application of POD low-order reconstruction and time-marching algorithm on the accuracy and efficiency of pressure field reconstruction and noise prediction using TR-PIV. The instantaneous pressure field was then reconstructed by solving the Poisson equation. The preliminary result provides a detailed assessment conducted for the tandem cylinder flow to demonstrate the effectiveness of the time-marching algorithm on accelerating computation and POD low-order reconstruction for precise pressure reconstruction and far-field noise prediction.

2. Methodology

2. 1 POD based low-order reconstruction

Sirovich improved the direct POD method into a snapshot POD method (Sirovich, 1987), reducing the correlation matrix from spatial to temporal dimension and enabling POD analysis for high spatial resolution PIV data. The velocity fluctuation $u(x, t)$ can be represented as a linear combination of spatial modes $\phi_n(x)$:

$$u(x,t) = \sum a_n(t)\phi_n(x) \tag{2}$$

From the POD perspective, the linear combination should be optimal. This can be accomplished by solving the eigenvalue problem of an autocovariance matrix, as detailed in (Wang, Cao, & Zhou, 2014). And POD low-order reconstruction can be expressed as:

$$U_s(x,t) = \overline{U} + \sum_{n=1}^{Tr} a_n(t)\phi_n(x) \tag{3}$$

where $U_S(x, t)$ is the POD low-order reconstructed velocity, $\overline{U}$ is the averaged velocity and Tr denotes the truncation modes for reconstruction.

2. 2 Pressure reconstruction from time-resolved PIV data

Firstly, the pressure gradient is derived from the incompressible Naviar-Stocks equation (1) in the Euler perspective. Material acceleration in (1) is divided into two parts:

$$\frac{DU}{Dt} = \frac{\partial U}{\partial t} + U \cdot \nabla U \tag{4}$$

The first and second term denote local and convective acceleration, respectively. Taking divergence of (1), ignoring the viscous term and considering the 2-dimensional divergence free condition, the Poisson equation can be derived (van Oudheusden, 2013):

$$\Delta P = \frac{\partial^2 P}{\partial x^2} + \frac{\partial^2 P}{\partial y^2} = -\rho\left\{\left(\frac{\partial U_x}{\partial x}\right)^2 + 2\frac{\partial U_y}{\partial x}\frac{\partial U_x}{\partial y} + \left(\frac{\partial U_y}{\partial y}\right)^2\right\} \tag{5}$$

Consequently, the source term of Poisson equation ΔP can be evaluated based on POD denoising velocity. Solving the Poisson equation is an iterative process that needs appropriate boundary conditions, an initial guess, and the numerical iterative scheme. Boundaries of FOV parallel to freestream are implemented Dirichlet boundary condition, enforcing pressure here through extended Bernoulli equation (R. de Kat & van Oudheusden, 2011):

$$P_{ref} + \frac{1}{2}\rho\left(\overline{U}\cdot\overline{U} + U'\cdot U'\right) = P_{\infty} + \frac{1}{2}\rho U_{\infty}^{2} \tag{6}$$

The inlet, outlet of FOV, and wall surface are Neumann boundaries, where the pressure gradient is prescribed with (1). Setting a time-marching initial guess, spatial pressure is evaluated with the SOR scheme. Finally, the wall pressure was determined by averaging the data integrated from the spatial pressure of the nearest nine PIV grid nodes to the discrete points on the wall surface (Jux et al., 2020):

$$P_w = \frac{1}{N_p}\sum_{i=1}^{i=N_p}\left(\nabla P_{i\to w} dx_{i\to w} + P_i\right) \tag{7}$$

where P_W is wall pressure, N_p is the number of nodes participating in integration, $\nabla P_{i\to w}$ is the pressure gradient and $dx_{i\to w}$ is the integration path.

2. 3 Far-field noise prediction

The far-field acoustic pressure Pa of a stationary, rigid solid surface immersed in a fluid field is composed of dipole related to solid surface loading and turbulence relative to quadrupole (Curle, 1955). Under low Mach number conditions, the quadrupole contribution is negligible and the far-field noise can be predicted with spanwise correction (Zhang, Sciacchitano, & Pröbsting, 2018).

3. Experimental Assessment of Tandem Cylinder

Tandem cylinder flow is ubiquitous in engineering and often occurs in scenarios such as heat exchangers, landing gear of airplanes, and high-speed rail pantographs (Yu Zhou & Mahbub Alam, 2016), which frequently suffer from vortex-induced vibration (VIV) and aerodynamic noise. Therefore, tandem cylinder flow is conducted as an assessment to demonstrate the benefit of POD low-order reconstruction and time-marching initial guesses in the present work.

The experiments were conducted in the anechoic wind tunnel of the Institute of Fluids Engineering at Zhejiang University. The cross-section of the test section is 0.4 × 0.5 m^2 with a turbulence intensity of less than 0.5%. A pair of circular cylinders arranged in tandem are installed in the symmetry plane of the test section, extending over the entire span. The diameter of cylinders (D) is 15 mm and the streamwise spacing between the cylinders (L) is 4.2D. The coordinate system centered at the downstream cylinder center is used. The freestream velocity is set at U_∞ = 8 m/s and 10 m/s, with Reynolds numbers based on cylinder diameter (Re_D) of 0.81 and 1.01 × 10^4.

TR-PIV is used to capture the instantaneous velocity fields. A high-speed laser (Vlite-Hi-50K, 2 × 50 mj per pulse at 1 kHz) was used to illuminate particles seeded with 1 μm DESH in the flow field. A Photron FASTCAM Mini camera AX100 (1024 pixel × 1024 pixel) equipped with Nikon 105mm prime objective is used to capture particle images. To increase temporal resolution, the camera sensor is cropped into 896 pixels × 608 pixels, resulting in an acquisition frequency (fs) of

4 kHz with 40 μs pulse separation. The FOV of the measurement is 80.9 mm × 54.9 mm ($x \times y$), with a digital image resolution of 11.1 pixel/mm. As the dominant sound source (Geyer, 2022), the downstream cylinder is located at the center of FOV (Fig.1 (b)). To avoid obstruction, the laser was divided into two equal beams by a 50% splitter and then expanded and thinned through an optics series to create two overlapping laser sheets of 1.5 mm thickness, enabling 360° cylinder illumination (Fig.1 (a)). The measurement was taken over a sampling time of 2 s, corresponding to 4000 image pairs. LaVision Davis 10.1 is used for PIV system synchronization, data acquisition, and processing. All particle images are cross-correlated with multiple iterations. The final integration window size of 16 pixels × 16 pixels with 75% overlap is applied, resulting in a vector pitch of 0.36 mm.

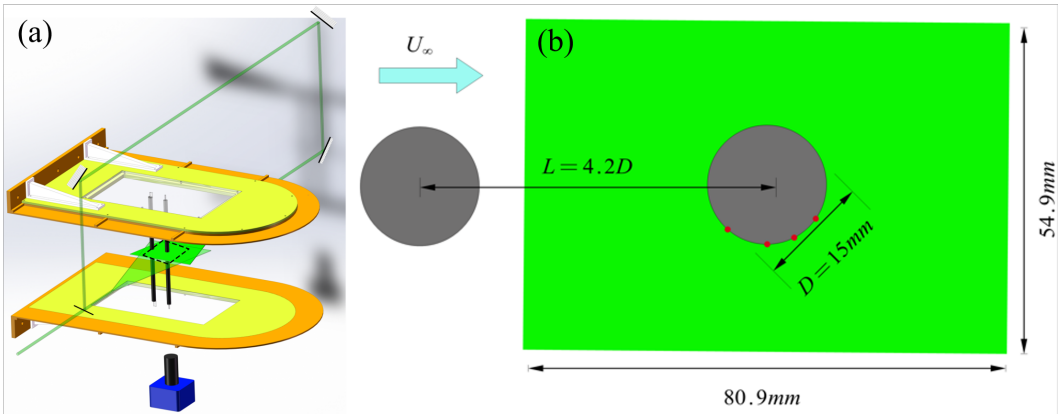

Fig.1 (a) PIV setup and (b) FOV of tandem cylinder flow

An additional spanwise planar PIV was performed over the x-z plane to supply spanwise correction of noise prediction, with FOV of 57 mm × 70 mm, corresponding to 640 pixels × 748 pixels and digital image resolution is 11.2 pixel/mm. The sampling frequency and time remain the same. Wall surface pressure fluctuation signals were simultaneously sampled by a miniature Knowles FG-23329-P07 transducer, mounted inside the downstream cylinder at the symmetry plane. The direction of the miniature transducer was adjusted by rotating the cylinder to $\alpha = 45°$, 90°, 120° and 150° as shown in Fig.1 (b) by the red points. The measurement was performed with a sampling frequency of 51.2 kHz simultaneously with PIV measurement. The supplementary far-field noise was measured by three G.A.R.S 40PH-10 CCP with a sampling frequency of 40 kHz over 30 s, located 1 meter away from the downstream cylinder with respect to the freestream direction of 75°, 90°, and 120°.

The turbulence intensity of the tandem cylinder flow is depicted in Fig.2 for $U_\infty = 8$ m/s and 10 m/s. In the present work, the tandem cylinder flow for $U_\infty = 8$ m/s is under a bi-stable state (Elhimer et al., 2016), where reattachment (Fig.2 (a)) and co-shedding (Fig.2 (b)) switch to each other randomly. while the co-shedding state (Fig.2 (c)) maintains stably for $U_\infty = 10$ m/s. Based on the turbulence intensity distribution, the boundaries can be classified. The top and bottom

boundaries of FOV with lower turbulence intensity are considered as Dirichlet boundaries, providing pressure here through equation (6). Conversely, the inlet, outlet of FOV, and surface of the cylinder are regarded as Neumann boundaries due to high turbulence intensity and are enforced pressure gradient through equation (1).

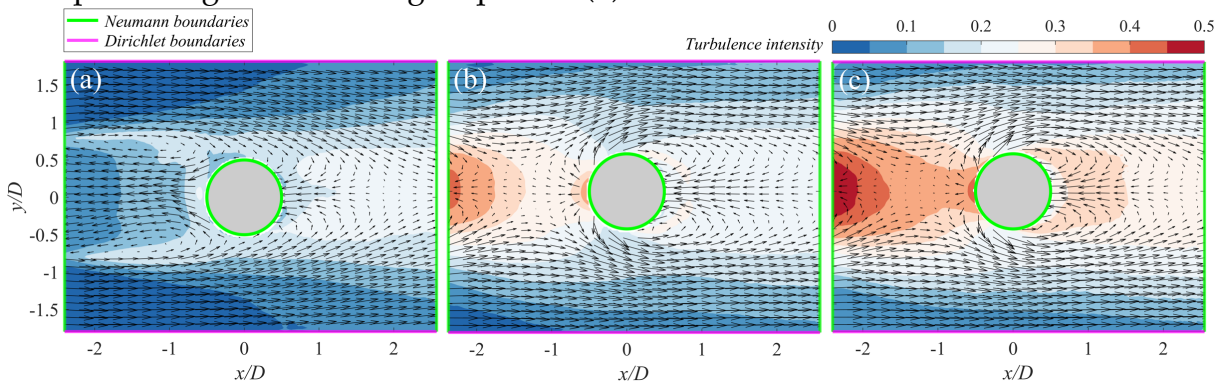

Fig.2 Turbulence intensity of (a) reattachment state for $U_\infty = 8$ m/s, (b) co-shedding state for $U_\infty = 8$ and (c) 10 m/s

4. Results

4. 1 Effect of POD based low-order reconstruction on pressure estimation

To ensure statistical convergence, POD analyses are performed using 2000, 3000, and 4000 snapshots. The energy content of the first 20 modes is almost identical, indicating that 4000 snapshots are sufficient for converging the POD analysis.

Further quantitative estimation of the random error of instantaneous velocity is performed through the noise level (flat part in high-frequency range) in the premultiplied PSD of velocity fluctuations (Sina Ghaemi et al., 2012). The premultiplied PSD of streamwise $f\Phi_{uu}$ and lateral velocity $f\Phi_{vv}$ at the free-stream (FOV top boundary) are shown in Fig.3. The results indicate a notable noise levels reduction after POD low-order reconstruction with 90% and 80% total disturbance energy. The total displacement error $\epsilon ds = \sqrt{(\epsilon dx^2 + \epsilon dy^2)}$ decreases from 0.142 to 0.021 pixels. The displacement error of free-stream after POD low-order reconstruction is much lower than 0.1 pixel reported in (R. de Kat & van Oudheusden, 2011). Meanwhile, Fig.3 also suggests that the POD low-order reconstruction can improve the cut-off frequency of velocity, especially for POD low-order reconstruction with 70% energy contribution.

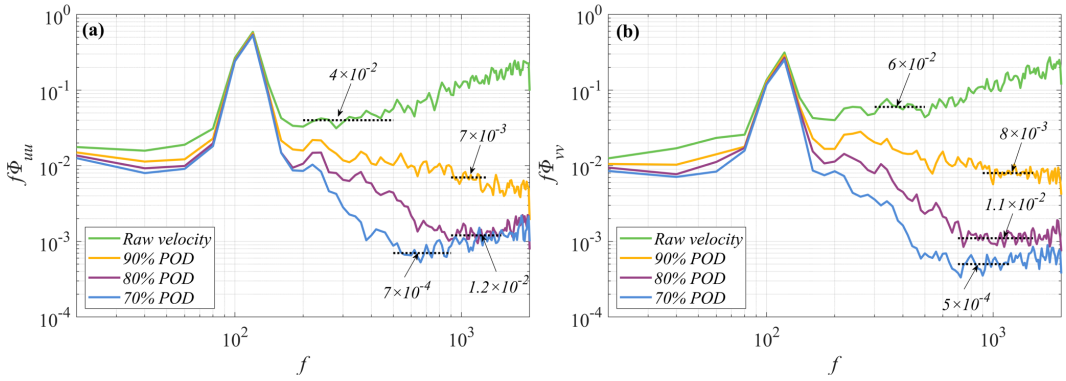

Fig.3 Premultiplied PSD of (a) streamwise velocity $f\Phi_{uu}$ and (b) lateral velocity $f\Phi_{vv}$ at free-stream (FOV top boundary)

Furthermore, the raw and low-order reconstructed velocity fields with 70%, 80%, and 90% energy contents are utilized as inputs into the Poisson solver to estimate pressure. Comparisons are made with the pressure signals simultaneously measured with the transducer at α = 150° for U_∞ = 8 and 10 m/s. The correlation curves between the pressure signal reconstructed and measured through the transducer are shown in Fig.4. The peak values receive great enhancement from 0.5 to 0.7 and 0.3 to 0.55 for U_∞ = 8 and 10 m/s, respectively. The results for POD low-order reconstruction of accounting for different mode energy display nearly identical results. Then, the power spectrum density of the normalized p'/p'_{rms} signal is estimated. The results (Fig.5) show that POD low-order reconstruction improves the agreement between the reconstructed pressure and reference signal, particularly in the high-frequency range.

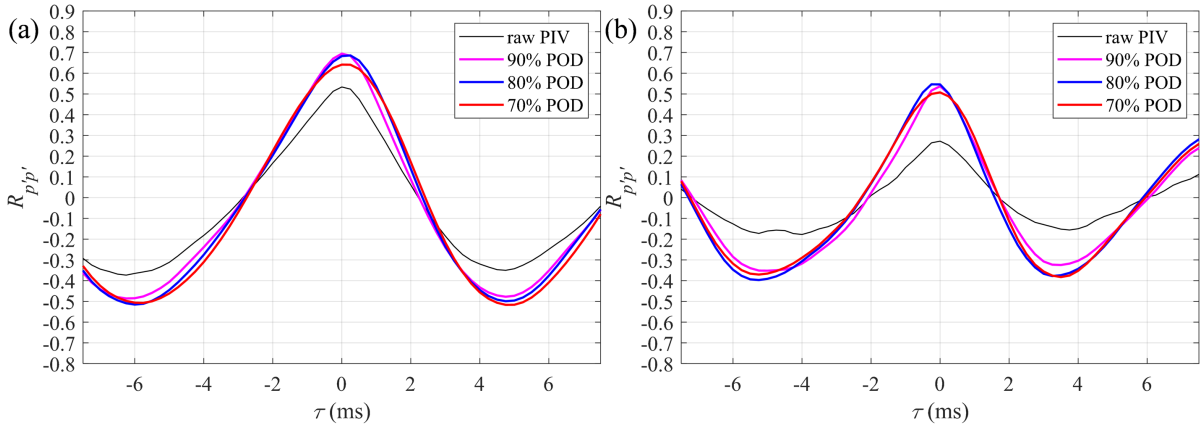

Fig.4 Correlation of pressure fluctuations $R_{P'P'}$ between estimated signals based on PIV and reference signals measured by pressure transducers at α = 150°. (a) U_∞ = 8 m/s, (b) U_∞ = 10 m/s

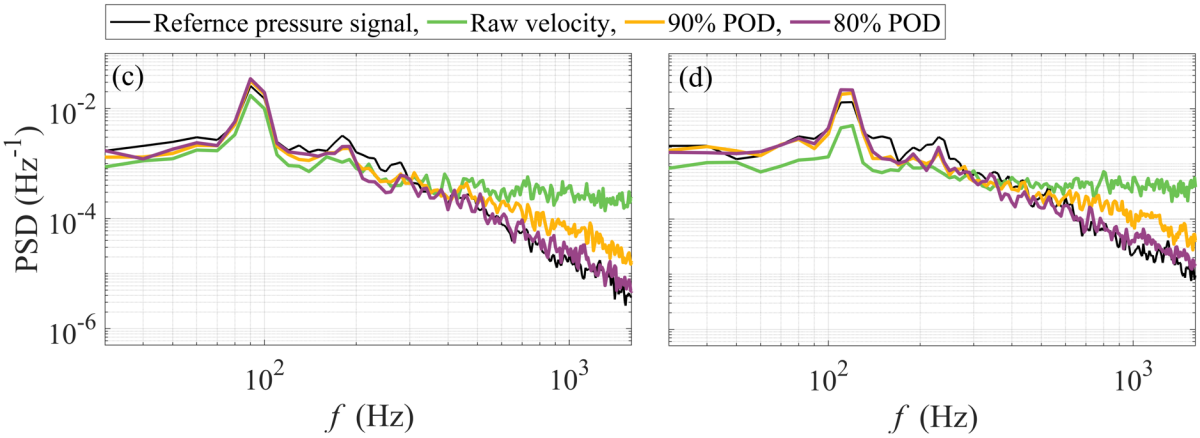

Fig.5 PSD of the estimated and reference pressure signals (p'/p'_{rms}) for (a) $U_\infty = 8$ and (b) $U_\infty = 10$ m/s

4. 2 Effect of time marching algorithm

As the source of the dipole, wall pressure fluctuations are the major contributor to the generation of far-field noise. Fig.6 illustrates the normalized wall-pressure deviation ((P_k-P)/(0.5ρU_∞^2)) of 72 dispersed points during iteration. where P_α is the pressure value in the k iteration step, P is the final convergence value and q refers to the dynamic pressure. Before reaching 1000 iterations, the iteration progress corresponding to the freestream initial guess performs chaotic and oscillating. On the contrary, the deviation decreases monotonically and fast for the time-marching initial guess. Setting the threshold deviation as 0.005, it is found that 1951 iterations are sufficient for convergence when using a time-marching initial guess, which is 32.7% faster than the 2897 iterations required for freestream initial guess. These results suggest that time-marching initial guess has advantages on convergent speed and stabilization during iteration. Stabilization during iterations also allows a radical β (closer to 2) employed in the SOR scheme, thereby again accelerating the convergence.

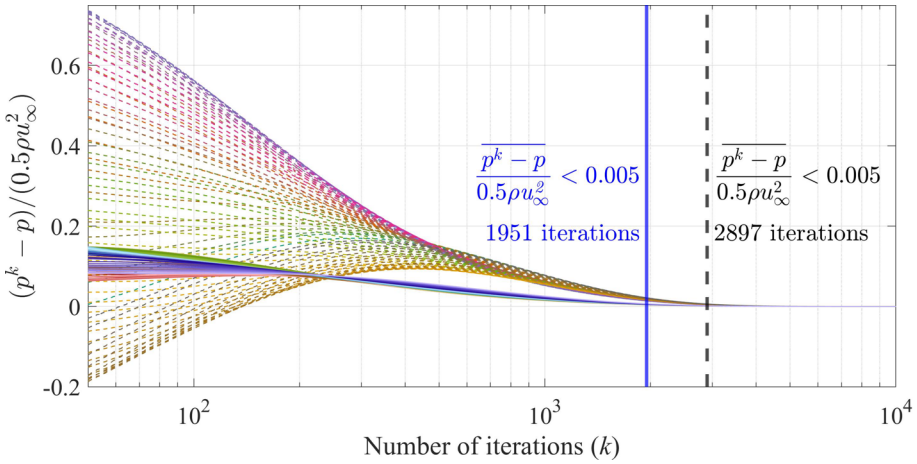

Fig.6 The normalized deviation between wall pressure and its converged value at various discrete points during the iterative updating process, solid and dot lines represent freestream and time-marching initial guess, respectively

4. 3 Assessment of far-field noise prediction

Finally, the reconstructed wall pressure is applied for far-field noise prediction through Curle's analogy considering spanwise correction, the noise results for the listener at 90°. Comparison with the reference far-field microphone is shown in Fig.7. The predicted noise based on various velocity inputs shows good agreement with noise measured with the microphone at the dominant and corresponding harmonic tonal peak. Particularly, noise derived from POD low-order reconstruction performs better in the high-frequency range, capturing the third harmonic tonal peak and slope in the mid- to high-frequency band similar to the reference in the high-frequency range.

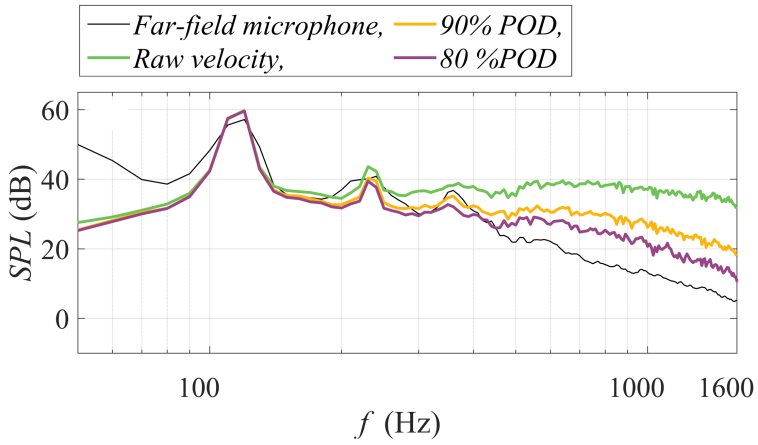

Fig.7 The predicted far-field noise for the listener at 90°

5. Conclusion

In the present work, we propose a fast and accurate approach for TR-PIV-based pressure reconstruction. By implementing POD low-order reconstruction for velocity field denoising and time-marching algorithm for accelerating the computation, the accuracy and efficiency of PIV-based pressure reconstruction are enhanced. These enhancements are assessed by considering a tandem cylinder flow with $Re_D = 0.81$ and 1.01×10^4. The flow fields and wall pressure of tandem cylinder flow were simultaneously measured with TR-PIV and a miniature Knowles transducer.

The POD low-order reconstruction is applied to remove the random errors and small-scale turbulence within the instantaneous velocity fields, thereby proving denoising input for solving the pressure Poisson equation. Both correlations and spectrum results demonstrate the enhancement of wall pressure accuracy by employing the POD low-order reconstruction. The time-marching enhancement algorithm is applied by using the reconstructed pressure field from the proceeded time instant as the initial guess of the current instant in the SOR scheme. The iteration steps to obtain data convergence of surface pressure are reduced by 32.6% compared with that using free-stream pressure as the initial guess. The final prediction on far-field noise is performed through Curle's analogy, considering the spanwise correlation correction. The POD-based denoising improves the accuracy for identifying the peaks of the total noise and broad-band noise compared with the reference measurement.

Acknowledgements

This research has been supported by the National Key R&D Program of China (Grant No: 2020YFA0405700), National Natural Science Foundation of China (Grant No: 12372280).

References

Azijli, I., Sciacchitano, A., Ragni, D., Palha, A., & Dwight, R. P. (2016). A posteriori uncertainty quantification of PIV-based pressure data. Experiments in Fluids, 57(5). doi:10.1007/s00348-016-2159-z

Curle, N. (1955). The influence of solid boundaries upon aerodynamic sound. Proceedings of the Royal Society of London. Series A. Mathematical and Physical Sciences, 231(1187), 505-514.

de Kat, R., & van Oudheusden, B. W. (2011). Instantaneous planar pressure determination from PIV in turbulent flow. Experiments in Fluids, 52(5), 1089-1106. doi:10.1007/s00348-011-1237-5

Fujisawa, N., Tanahashi, S., & Srinivas, K. (2005). Evaluation of pressure field and fluid forces on a circular cylinder with and without rotational oscillation using velocity data from PIV measurement. Measurement Science and Technology, 16(4), 989-996. doi:10.1088/0957-0233/16/4/011

Ghaemi, S., & Scarano, F. (2013). Turbulent structure of high-amplitude pressure peaks within the turbulent boundary layer. Journal of Fluid Mechanics, 735, 381-426. doi:10.1017/jfm.2013.501

Jux, C., Sciacchitano, A., & Scarano, F. (2020). Flow pressure evaluation on generic surfaces by robotic volumetric PTV. Measurement Science and Technology, 31(10). doi:10.1088/1361-6501/ab8f46

Pan, Z., Whitehead, J., Thomson, S., & Truscott, T. (2016). Error Propagation Dynamics of PIV-based Pressure Field Calculations: How well does the pressure Poisson solver perform inherently? Meas Sci Technol, 27(8), 084012. doi:10.1088/0957-0233/27/8/084012

Ragni, D., Avallone, F., van der Velden, W. C. P., & Casalino, D. (2018). Measurements of near-wall pressure fluctuations for trailing-edge serrations and slits. Experiments in Fluids, 60(1). doi:10.1007/s00348-018-2654-5

Ragni, D., Fiscaletti, D., & Baars, W. J. (2022). Jet noise predictions by time marching of single-snapshot tomographic PIV fields. Experiments in Fluids, 63(5). doi:10.1007/s00348-022-03436-3

Sirovich, L. (1987). Turbulence and the dynamics of coherent structures. I. Coherent structures. Quarterly of applied mathematics, 45(3), 561-571.

van Oudheusden, B. W. (2013). PIV-based pressure measurement. Measurement Science and Technology, 24(3). doi:10.1088/0957-0233/24/3/032001

Wang, H. F., Cao, H. L., & Zhou, Y. (2014). POD analysis of a finite-length cylinder near wake. Experiments in Fluids, 55(8). doi:10.1007/s00348-014-1790-9

Zhang, X., Sciacchitano, A., & Pröbsting, S. (2018). Aeroacoustic analysis of an airfoil with Gurney flap based on time-resolved particle image velocimetry measurements. Journal of Sound and Vibration, 422, 490-505. doi:10.1016/j.jsv.2018.02.039

Zhou, Y., & Mahbub Alam, M. (2016). Wake of two interacting circular cylinders: A review. International Journal of Heat and Fluid Flow, 62, 510-537. doi:10.1016/j.ijheatfluidflow.2016.08.008